Structural insights into WHAMM-mediated cytoskeletal coordination during membrane remodeling

Qing-Tao Shen,[1] Peter P. Hsiue,[2] Charles V. Sindelar,[1] Matthew D. Welch,[2] Kenneth G. Campellone,[2,3] and Hong-Wei Wang[1,4,5]

[1]Department of Molecular Biophysics and Biochemistry, Yale University, New Haven, CT 06520
[2]Department of Molecular and Cell Biology, University of California, Berkeley, Berkeley, CA 94720
[3]Department of Molecular and Cell Biology, University of Connecticut, Storrs, CT 06269
[4]Tsinghua-Peking Center for Life Sciences, Tsinghua University, Beijing, China 100084
[5]Center for Structural Biology, School of Life Sciences, Tsinghua University, Beijing, China 100084

The microtubule (MT) and actin cytoskeletons drive many essential cellular processes, yet fairly little is known about how their functions are coordinated. One factor that mediates important cross talk between these two systems is WHAMM, a Golgi-associated protein that utilizes MT binding and actin nucleation activities to promote membrane tubulation during intracellular transport. Using cryoelectron microscopy and other biophysical and biochemical approaches, we unveil the underlying mechanisms for how these activities are coordinated. We find that WHAMM bound to the outer surface of MT protofilaments via a novel interaction between its central coiled-coil region and tubulin heterodimers. Upon the assembly of WHAMM onto MTs, its N-terminal membrane-binding domain was exposed at the MT periphery, where it can recruit vesicles and remodel them into tubular structures. In contrast, MT binding masked the C-terminal portion of WHAMM and prevented it from promoting actin nucleation. These results give rise to a model whereby distinct MT-bound and actin-nucleating populations of WHAMM collaborate during membrane tubulation.

Introduction

The microtubule (MT) and actin cytoskeletons organize the mammalian cell cytoplasm and have well-established roles in many dynamic processes, including cell division, migration, morphogenesis, and membrane trafficking. MTs and their motor proteins are especially crucial for mitosis (Dumont and Mitchison, 2009; Gatlin and Bloom, 2010) and vesicle transport (Brownhill et al., 2009), whereas actin and its motor proteins are best known for generating the protrusive and contractile forces that control cell shape, motility, and cytokinesis (Pollard and Cooper, 2009). Actin also has important functions in endocytosis (Kaksonen et al., 2006; Galletta et al., 2010). Importantly, despite the fact that much is known about how MTs and actin filaments operate as distinct entities, relatively little is understood about how these two cytoskeletal systems are coordinated. In particular, the mechanisms by which MTs and actin cooperate during the remodeling and transport of membranes that function in the secretory pathway remain to be established.

In recent years, a great deal of attention has been focused on elucidating the forces and factors that drive membrane shape changes (Shibata et al., 2009), and current evidence indicates that actin filament assembly initiated by molecules called nucleators is key for controlling cell and organelle morphogenesis. In mammalian cells, multiple classes of actin nucleators promote filament polymerization. These include 15 formin family proteins and a variety of actin monomer-clustering proteins that generate unbranched filaments as well as eight Wiskott–Aldrich syndrome protein (WASP) family nucleation-promoting factors (NPFs) that act in concert with the Arp2/3 complex to

Correspondence to Hong-Wei Wang: hongweiwang@tsinghua.edu.cn; or Kenneth G. Campellone: kenneth.campellone@uconn.edu

Abbreviations used in this paper: CC, coiled coil; FFT, fast Fourier transform; MBP, maltose-binding protein; MT, microtubule; NPF, nucleation-promoting factor; NTA, nitrilotriacetic acid; PIP, phosphatidylinositol phosphate; TEV, tobacco etch virus; WASH, WASP and SCAR homologue; WASP, Wiskott–Aldrich syndrome protein; WMD, WHAMM membrane-interacting domain.

The Rockefeller University Press $30.00
J. Cell Biol. Vol. 199 No. 1 111–124
www.jcb.org/cgi/doi/10.1083/jcb.201204010

create branched filament networks (Campellone and Welch, 2010; Chesarone et al., 2010). Several of these NPFs collaborate with membrane-binding proteins from the BAR (Bin–Amphiphysin–Rvs) and/or dynamin families to cause remodeling of lamellipodia and endosomes (Qualmann et al., 2011; Ferguson and De Camilli, 2012).

Among this cohort of >30 proteins with direct roles in actin nucleation, only a few are known to physically interact with MTs. The best examples are the formins mDia1, mDia2, and INF2, which have all been shown to nucleate actin (although with different potency) and bind to MTs (albeit with different biochemical properties; Bartolini et al., 2008; Gaillard et al., 2011). mDia1 and mDia2 participate in actin assembly within lamellipodia and filopodia (Yang et al., 2007), whereas INF2 appears to influence the ER morphology and Golgi organization (Ramabhadran et al., 2011). However, the actual role of MT binding by formins during these membrane rearrangements is not clear.

In contrast to the observations that multiple formins can bind MTs, only one of the mammalian NPFs—WHAMM—has been shown to physically interact with MTs in cells and in vitro (Campellone et al., 2008). WHAMM also localizes to membranes of the ER-Golgi intermediate compartment and the cis-Golgi apparatus, and it can bind to phospholipids (Campellone et al., 2008). The cellular secretory system consists of organelles with diverse shapes ranging from the complex tubular network of the ER (Hu et al., 2011) to stacked Golgi cisternae (Lowe, 2011) and to pleomorphic vesicular and tubular cargo carriers that move between these compartments (Polishchuk et al., 2009; Saraste et al., 2009), and WHAMM appears to influence both the structure and function of this system. WHAMM is important for maintaining Golgi organization near the centrosome, for the formation of tubular membranes that move from the ER to the Golgi, and for efficient anterograde transport (Campellone et al., 2008).

Like all WASP family NPFs, WHAMM has a C terminus termed the PWCA region that consists of a proline-rich peptide and WH2 motifs that bind actin monomers plus connector and acidic segments that interact with the Arp2/3 complex. However, WHAMM can be distinguished from other NPFs by the fact that it possesses a unique N terminus called the WHAMM membrane-interacting domain (WMD) and a long central coiled-coil (CC) domain (Campellone et al., 2008). These two domains mediate the interaction of WHAMM with phospholipids and MTs, respectively. Mutagenesis and chemical inhibitor experiments suggest that membrane association, MT binding, and actin nucleation are all crucial for WHAMM to generate and maintain membrane tubules, but how these three activities are coordinated is not known (Campellone et al., 2008).

In this study, we combined in vitro biochemical assays with cryo-EM reconstructions to provide new insights into how MTs influence actin filament assembly and WHAMM-mediated membrane remodeling. We found that the WHAMM CC domain engaged MTs specifically along the heterodimeric tubulin lattice. The MT-bound conformation of WHAMM allowed its WMD to recruit membranes but prevented its PWCA region from promoting actin nucleation. Thus, our work reveals an initial view of how a CC domain can interact with MTs, and it also explains how MT binding, membrane association, and actin nucleation are coordinated during WHAMM function.

Results

The CC domain of WHAMM binds to MTs along individual protofilaments

WHAMM can physically interact with MTs, yet how this association is coordinated with its membrane-binding and actin nucleation activities is not understood. To address this question, we first sought to characterize the interactions between WHAMM and MTs. We have shown previously that an N-terminally His-tagged version of full-length WHAMM and a GST-tagged derivative of the CC domain bind to taxol-stabilized MTs in cosedimentation assays in vitro (Campellone et al., 2008). However, the His- and GST-tagged proteins could only be purified in a soluble form in limited amounts. Therefore, we developed a maltose-binding protein (MBP) tagging system for expressing high levels of soluble WHAMM fusion proteins in insect cells (see Materials and methods). We then purified MBP-WHAMM by successive amylose affinity and gel filtration chromatography steps. Full-length His-WHAMM (Campellone et al., 2008) and MBP-WHAMM exhibited equivalent nucleation-promoting activities in pyrene-actin polymerization assays (unpublished data), but the MBP-tagged protein could be purified in much larger quantities, so we used MBP-WHAMM and its derivatives (diagrammed in Fig. 1 A) to investigate the biochemical and structural characteristics of the interactions between WHAMM and MTs.

To begin to examine the MT-binding properties of WHAMM, we assembled taxol-stabilized MTs from purified tubulin heterodimers and performed cosedimentation assays with MBP fusion proteins containing either full-length WHAMM or different WHAMM truncations (Fig. 1, A and B). (For simplicity, we will omit the abbreviation MBP when discussing these constructs in the rest of the paper.) These experiments demonstrated that all proteins containing the CC domain bound to MTs, whereas MBP alone and fusions containing just the WMD or PWCA domain did not (Fig. 1 B).

To measure the affinity and stoichiometry with which WHAMM engages MTs, we performed cosedimentation assays using full-length WHAMM, its isolated CC domain, and MTs at a range of concentrations. WHAMM bound to MTs with a dissociation constant of 405 nM (Fig. 1 C), indicating that this interaction occurs with a fairly high affinity. At saturation, the molar ratio between WHAMM and tubulin heterodimers was ∼1:1 (Fig. 1 D). The CC domain also bound to MTs at 1:1 stoichiometry but with a twofold higher affinity than full-length WHAMM (Fig. 1, E and F).

To reveal the molecular details of the interactions between WHAMM and MTs, we examined complexes of MT with WHAMM (WHAMM::MT) and CC (CC::MT) by EM. Under both negative staining and vitrification conditions, MTs incubated with WHAMM or CC became thicker with obvious additional densities decorating the MT outer surface (Fig. 2, A and B). A WHAMM-decorated MT had a diameter of 40 nm compared

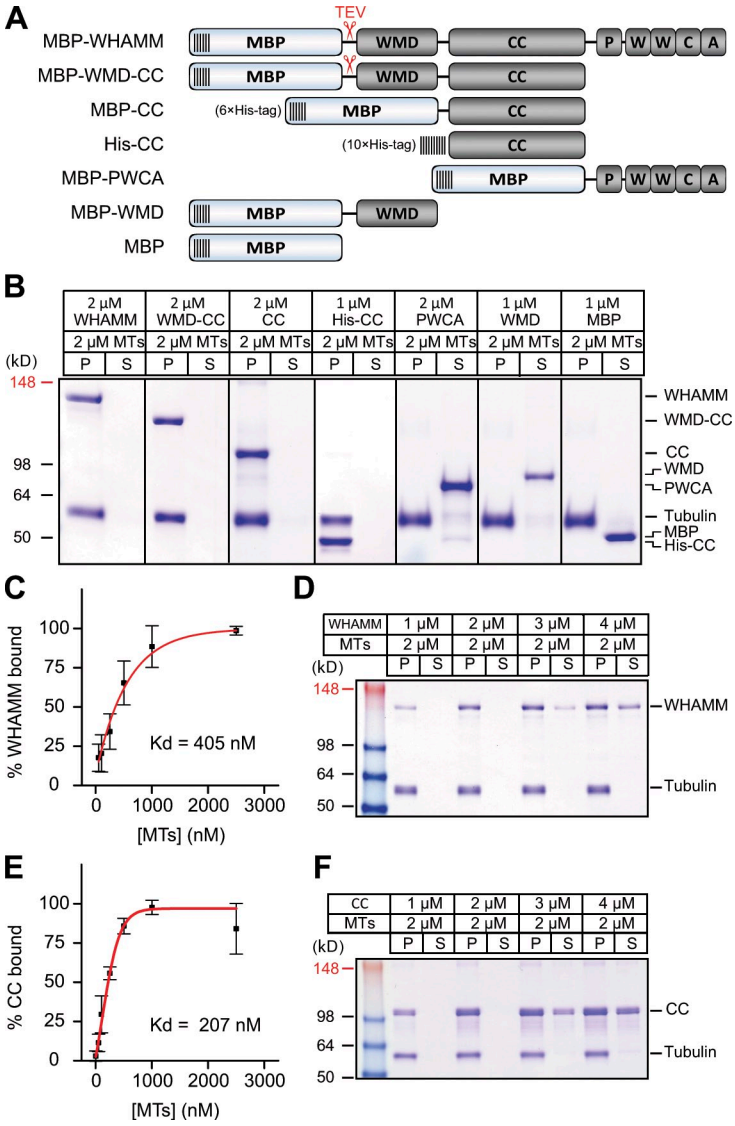

Figure 1. **The CC domain of WHAMM binds to MTs at a 1:1 WHAMM/tubulin heterodimer ratio with high affinity.** (A) The domain organization of maltose-binding protein (MBP)– and polyhistidine (His)-tagged WHAMM derivatives that were used in this study are shown. TEV protease cleavage sites are highlighted in red. (B) Microtubule (MT) cosedimentation assays were performed using the indicated concentrations of MBP- or His-WHAMM fusion proteins and polymerized tubulin heterodimers. A representative Coomassie blue–stained gel of the pellet (P) and supernatant (S) fractions is shown. (C) Cosedimentation assays were performed using 100 nM MBP-WHAMM and various concentrations of polymerized tubulin heterodimers. (D) Cosedimentation assays were performed using various concentrations of MBP-WHAMM and 2 μM polymerized tubulin heterodimers. A representative Coomassie blue–stained gel is shown. The stoichiometry between MBP-WHAMM and tubulin heterodimers was ∼1:1 at saturation. (E) Cosedimentation assays using 100 nM MBP-CC were performed as in C. (F) Cosedimentation assays using MBP-CC were performed as in D and also revealed a ∼1:1 stoichiometry of CC to tubulin heterodimers. The red lines in C and E are fitted curves to the original data. Error bars show the range of data, which is calculated by subtracting the lowest value from the highest value.

with 24 nm for naked MTs (Fig. 2, C–E). Interestingly, we observed that at less than saturating concentrations of WHAMM, some MTs were fully decorated, whereas others remained naked (Fig. 2, A and B). A similar decoration pattern has also been observed for kinesin::MT complexes (Wendt et al., 2002).

When MTs polymerize in vitro, tubulin heterodimers align end to end to form a protofilament, and intact MTs typically assemble from 13–14 protofilaments. Notably, we observed examples of WHAMM::MT complexes in which only one side of the MT was decorated with WHAMM (Fig. 2 F), implying that some type of cooperativity might occur during WHAMM assembly along single protofilaments, a phenomenon that has also been seen for kinesin-decorated MTs (Wendt et al., 2002). The 1:1 stoichiometry that we observed in cosedimentation assays was also consistent with the possibility that WHAMM interacts with MTs along their heterodimeric tubulin lattice. To explore whether this was the case, we examined Fourier transforms of the electron micrographs of vitrified MTs that were fully decorated with WHAMM. In contrast to a naked MT, which only showed layer lines at 1/40 $Å^{-1}$ corresponding to tubulin monomers, the WHAMM-decorated MTs showed clear layer lines at 1/80 $Å^{-1}$, suggesting that WHAMM can differentiate α- and β-tubulin (Fig. 2 B).

Using single-particle approaches as in the analysis of other MT-binding proteins (Ramey et al., 2011b), we obtained 2D class averages of decorated MTs that displayed WHAMM densities on their outer surface (Fig. 2, D and E; and Fig. S1, A and B). WHAMM appeared bound to the periphery of tubulin heterodimers with a thin connection and a repeat of 80 Å along protofilaments. At larger radial distances, WHAMM densities enlarged and connected with each other along the protofilaments. Both 13- and 14-protofilament MTs were decorated, and Fourier transforms of their 2D class averages all showed a clear 1/80 $Å^{-1}$ signal (Fig. 2, D and E). This analysis agreed very well with the 1:1 stoichiometry observed in binding assays.

To preclude the possibility that the MBP tag affects this organization of WHAMM around MTs, we took advantage of the fact that a tobacco etch virus (TEV) protease cleavage site lies between the MBP tag and WHAMM in our fusion construct (Fig. 1 A) by developing an on-MT cleavage assay to remove

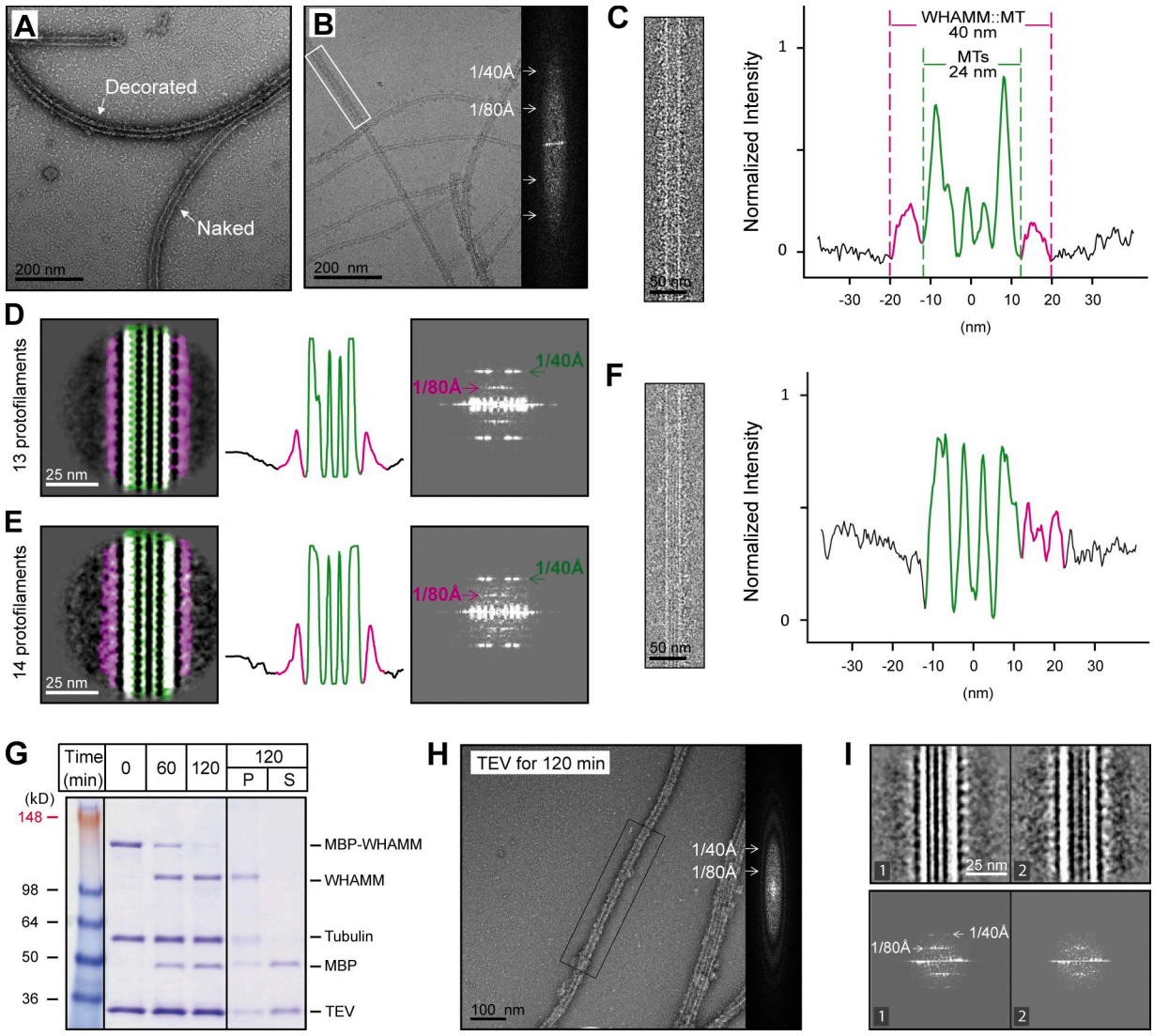

Figure 2. **WHAMM forms helical structures along MTs.** (A) A negative stain electron micrograph of a MBP-WHAMM::MT complex is shown. One MT was naked, whereas the other was decorated with WHAMM. (B) A cryoelectron micrograph of a MBP-WHAMM::MT complex and a FFT analysis of a selected complex is shown. The right image shows the existence of 40- and 80-$Å^{-1}$ layer lines. (C) A representative cryo-EM image of a MBP-WHAMM::MT complex was selected, and its diameter was calculated and labeled based on the known diameter of a 13-protofilament MT in a 1D projection profile on the right. The complex was increased in diameter compared with naked MTs. The MT is highlighted in green, and bound WHAMM is purple. (D and E) Two representative class averages from MBP-WHAMM::MT complexes, their respective 1D projection profiles, and respective power spectrums are shown. 13- and 14-protofilament MTs were discriminated by their moiré patterns. In the power spectrums, 40- and 80-$Å^{-1}$ layer lines are marked in colors as in C. (F) A representative cryo-EM image of MTs partially decorated with MBP-WHAMM is shown, and its 1D projection profile was calculated. WHAMM bound to protofilaments on one side of the MT. (G) MBP-WHAMM::MT complexes were treated with the TEV protease for the indicated times and analyzed directly by SDS-PAGE or were separated into pellet (P) and supernatant (S) fractions before SDS-PAGE analyses. Black lines indicate that intervening lanes have been spliced out. (H) Negatively stained EM images with a representative FFT analysis is shown for MBP-WHAMM::MTs that were cleaved with TEV protease. (I) Representative 2D class averages and respective power spectrums for the cleaved complexes are shown. In B and H, boxes are to box filaments for FFT analysis, the results of which are shown on the right.

the MBP moiety from WHAMM::MT complexes. The MBP-WHAMM junction was cleaved efficiently by the TEV protease after a 2-h incubation, and although WHAMM remained in the MT-associated pellet fraction, most of the MBP was liberated into the supernatant (Fig. 2 G). Negative staining EM of the cleaved WHAMM::MT complexes demonstrated that the 80-Å layer line was still visible (Fig. 2 H). To see this more clearly, we took the vitrified images of the cleaved WHAMM::MT complexes and obtained the 2D class averages. Clear additional density maps around MTs and the corresponding 80-Å layer lines were visible (Fig. 2 I), indicating that MBP is not necessary for maintaining a helical WHAMM orientation around MTs. To further confirm this, we examined the effect of TEV protease cleavage on MT decoration by another MBP-WHAMM fusion construct, WMD-CC. This construct bound to MTs with an affinity similar to the CC domain alone, and the on-MT cleavage reaction resulted in the specific removal of MBP from the pellet fraction without perturbing the MT-bound state of WMD-CC (Fig. S2, A–D). Moreover, when MBP-WMD-CC was cleaved in solution before the addition of MTs, cosedimentation assays and negative staining EM demonstrated that WMD-CC by itself bound to MTs (Fig. S2, A–D). Collectively, these results show that

MBP does not have a significant influence on the MT-binding properties of WHAMM.

Interestingly, when we analyzed CC-decorated MTs, we found densities along protofilaments following the heterodimeric tubulin lattice, but we did not observe the more peripheral structures that we saw with full-length WHAMM (Fig. S3, A–C). The shape of the CC density very closely resembled the one that was connected to the MT in the WHAMM::MT complex. These results confirmed that the CC domain is mainly responsible for the physical interaction of WHAMM with MTs, and they reemphasized that WHAMM can assemble along individual protofilaments. This latter property appears to be a characteristic that WHAMM shares with kinesin motor proteins (Harrison et al., 1993).

A 3D reconstruction of WHAMM on MTs

Because WHAMM decorates the heterodimeric tubulin lattice in a similar fashion to kinesins, we next sought to reconstruct the WHAMM::MT complex in 3D using the same algorithm that was used for the reconstruction of a kinesin::MT complex (Sindelar and Downing, 2007). We filtered the 3D map of 13-protofilament MTs decorated by kinesin-I to ∼30 Å and used it as an initial model to sort and align the segmented WHAMM::MT images. Through iterative alignment and refinement, we obtained a stable solution at an ∼18-Å resolution from 200 13-protofilament MTs in 77 micrographs after 12 iterations. These MTs showed clear 20-Å layer line signals after alignment (Fig. S4, A–D). The 3D reconstruction displayed a well-resolved shape of an MT and obvious additional densities protruding outwards from the MT surface (Fig. 3, A–C). The additional protrusion had a strikingly different shape from the kinesin structure, ruling out model bias in the refinement (Fig. S4 E). The bias-free nature of the refinement procedure has also been verified in other systems (Sindelar and Downing, 2007). Consistent with this, we used exactly the same method to obtain a 3D reconstruction from naked 13-protofilament MTs and did not see any additional densities on MT's outer surface (Fig. S4 F).

In the 3D map of the WHAMM::MT complex, a U-shaped density composed of two distinct parts was attached to the tubulin heterodimer (Fig. 3 A). One part had a globular shape and was connected to the outer ridge of a tubulin subunit via a linker density (Fig. 3 B). The other part had an elongated shape, was farther away from the MT surface, and did not contact the MT (Fig. 3 C). In addition, the U-shaped WHAMM molecule on one tubulin heterodimer did not appear to interact with neighboring WHAMMs on adjacent protofilaments (Fig. 3 C). Instead, WHAMM molecules on the same protofilament virtually connected with each other in a head to tail manner via their elongated densities (Fig. 3 B, black arrowhead).

Using the same aforementioned strategy, we also reconstructed the CC::MT complex at a resolution of 22 Å. To do this, we performed reconstructions of MTs decorated with MBP-CC and with His-CC (Fig. 1 A), a derivative that lacks the MBP tag and still binds to MTs at 1:1 stoichiometry (Fig. 1 B and not depicted). Each analysis yielded very similar results (Fig. 4, A–C; and not depicted). The His-CC domain decorated MTs in a nearly identical way to full-length WHAMM, with the same

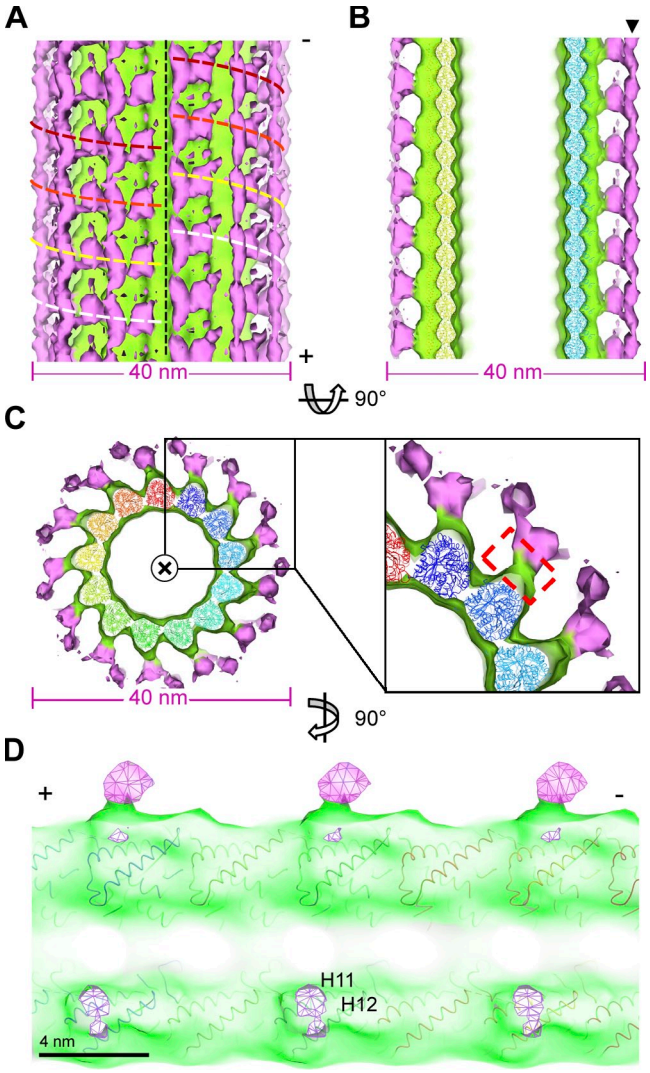

Figure 3. **3D reconstructions of WHAMM::MT complexes demonstrate the head to tail assembly of WHAMM along individual protofilaments.** (A) An isosurface view of MBP-WHAMM in complex with a 13-protofilament MT is shown. The MT is colored green, and bound WHAMM is purple. The vertical black dashed line indicates the MT seam. The colored dashed lines highlight the helical paths of WHAMM from each turn. The threshold of the isosurface display is adjusted to 0.045 (σ 1.62) to match the volume of the visible WHAMM density (190 nm^3) to the molecular mass of the MBP-WHAMM (136 kD). The positive and negative ends of the MT are also indicated. (B) A sliced orthogonal view of the MBP-WHAMM::MT complex is shown. The black triangle indicates potentially interacting parts between neighboring MBP-WHAMMs. (C) The sliced end-on (from the minus end) view of the MBP-WHAMM::MT complex and the fitting of pseudoatomic 13-protofilament MTs into the density maps is shown. In the zoomed quarter portion, the region of connection between one WHAMM and the MT is marked using a red dashed rectangle. (D) Helix 11 and helix 12 from the tubulin E-hook region are highlighted in this interface-capping model of the MBP-WHAMM::MT.

linker density and a similar, albeit smaller, globular density attached to the tubulin heterodimer. A difference map between the WHAMM::MT and CC::MT complexes showed that the major difference was that CC::MT lacked the elongated peripheral domain and a portion of the structure packed closely to the CC domain (Fig. 4, D and E).

Next, we docked the pseudoatomic model of a 13-protofilament MT (Li et al., 2002) into the WHAMM::MT and CC::MT

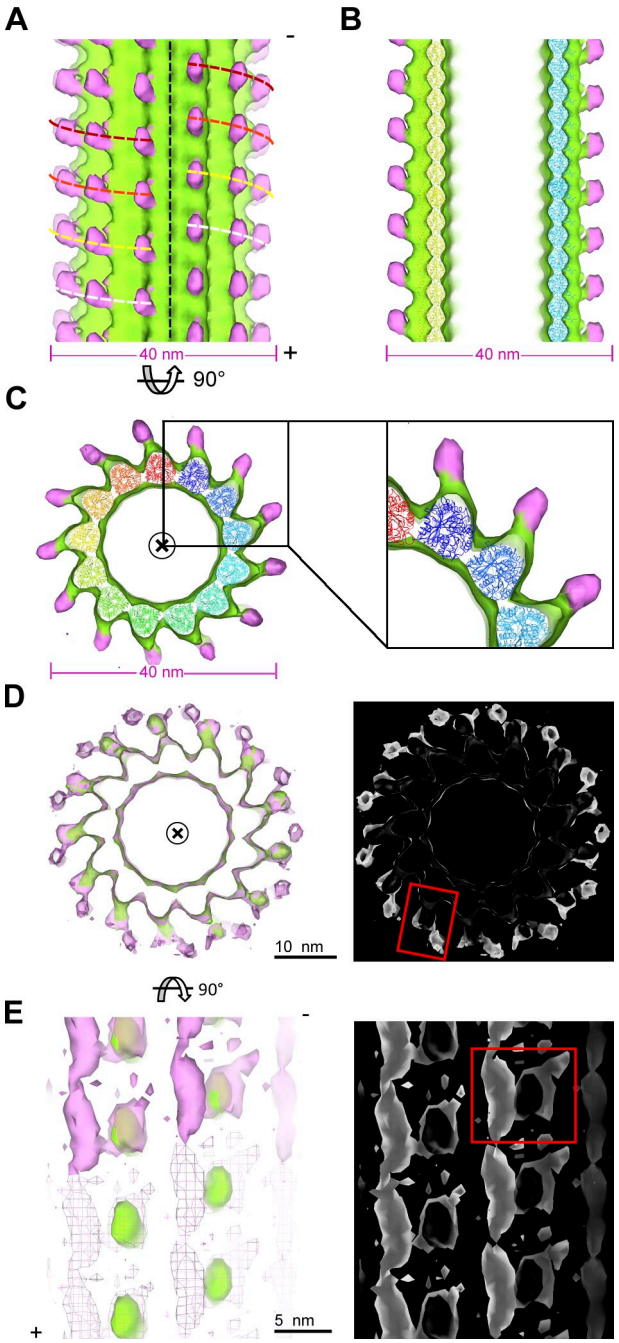

Figure 4. **3D reconstructions of His-CC::MT complexes reveal structural differences from WHAMM::MT complexes.** (A) An isosurface view of His-CC in complex with a 13-protofilament MT is shown. The MT is colored green, and bound His-CC is purple. The black dashed line indicates the MT seam. The horizontal dashed lines highlight the helical path of CC in each turn. (B) A sliced orthogonal view of the His-CC::MT complex is shown. (C) The sliced end-on (from the minus end) view of the His-CC::MT complex and the fitting of pseudoatomic 13-protofilament MTs into the density maps is shown. The 3D reconstruction of MBP-CC in complex with a 13-protofilament MT was virtually identical to those shown in A–C (not depicted), suggesting that the MBP moiety is flexible and was averaged out in the reconstruction process. The resolution of the His-CC::MT complex was estimated to be 22 Å based on RMEASURE. (D and E) Superimposition of WHAMM::MT and His-CC::MT and their difference maps are depicted in end-on and side views. In the left images, the WHAMM::MT complex is colored purple, and His-CC::MT is green. In the right images, one WHAMM molecule is marked in the red rectangles.

3D maps (unambiguously with a cross-correlation coefficient of 0.95), so we could examine the linker density between WHAMM and MTs more closely (Fig. 3, C and D). The linker density emanates from the end of tubulin helices 11 and 12, close to the C-terminal tubulin tail, which is a highly negatively charged polypeptide region termed the E-hook (Redeker et al., 1992). Interestingly, many MT-associated proteins are known to bind MTs through electrostatic interactions with E-hooks (Lakämper and Meyhöfer, 2005; Zanic et al., 2009; Ramey et al., 2011a). Moreover, the WHAMM CC domain has 72 basic residues in 371 amino acids and an estimated isoelectric point of 8.3, suggesting that it might interact with MTs electrostatically.

To examine this possibility, we tested whether high salt conditions could prevent WHAMM or CC from binding to MTs in cosedimentation assays. Indeed, increasing the amount of NaCl in the assays resulted in less WHAMM and CC bound to MTs. 250 mM NaCl caused a 50% reduction in the amount of WHAMM that bound to MTs, whereas 500 mM NaCl reduced binding by ∼90% (Fig. 5, A and B). To further explore the potential interaction between WHAMM and tubulin E-hooks, we treated MTs with subtilisin, a protease that can specifically remove the β-tubulin E-hooks from MTs under controlled conditions (Wang and Nogales, 2005). WHAMM binding to subtilisin-cleaved MTs was similar to WHAMM binding to untreated MTs (except for a small decrease in the percentage of bound protein at saturation), and it did not significantly alter the decoration morphology (Fig. 5, C and D). These results indicate that the E-hooks on β-tubulin are not required for binding WHAMM and therefore imply that WHAMM can interact with the remaining E-hooks present on α-tubulins.

MT-associated WHAMM can recruit and remodel membrane vesicles

Our description of the manner in which the central CC region of WHAMM assembles along protofilaments and engages tubulin heterodimers led us to explore how the other two major portions of WHAMM—the N-terminal WMD and C-terminal PWCA domain—are positioned when WHAMM is in its MT-bound state. The elongated density on the periphery of the WHAMM::MT complex is a major structure that the CC::MT complex lacks, and it should therefore correspond to the WMD or PWCA domain or both. The WMD has a longer primary sequence and is predicted to have more complex secondary structure than the PWCA domain, so we hypothesized that the peripheral density was mainly composed of the WMD. A 6×His peptide is at the N terminus of our MBP moiety (Fig. 1 A), and this tag should be accessible from solution in the WHAMM::MT complex if this portion of the protein comprises the peripheral density. To test this possibility, we incubated the WHAMM::MT complex with Ni-nitrilotriacetic acid (NTA)–conjugated gold particles. Consistent with the idea that the WMD is accessible on the surface of MTs, gold particles labeled structures emanating from the WHAMM::MT complex but distributed randomly in samples containing naked MTs (Fig. S5 A).

A GFP-tagged version of the WMD localizes to Golgi membranes in cells, and a His-tagged WMD interacts with multiple phospholipids, especially phosphatidylinositol phosphates

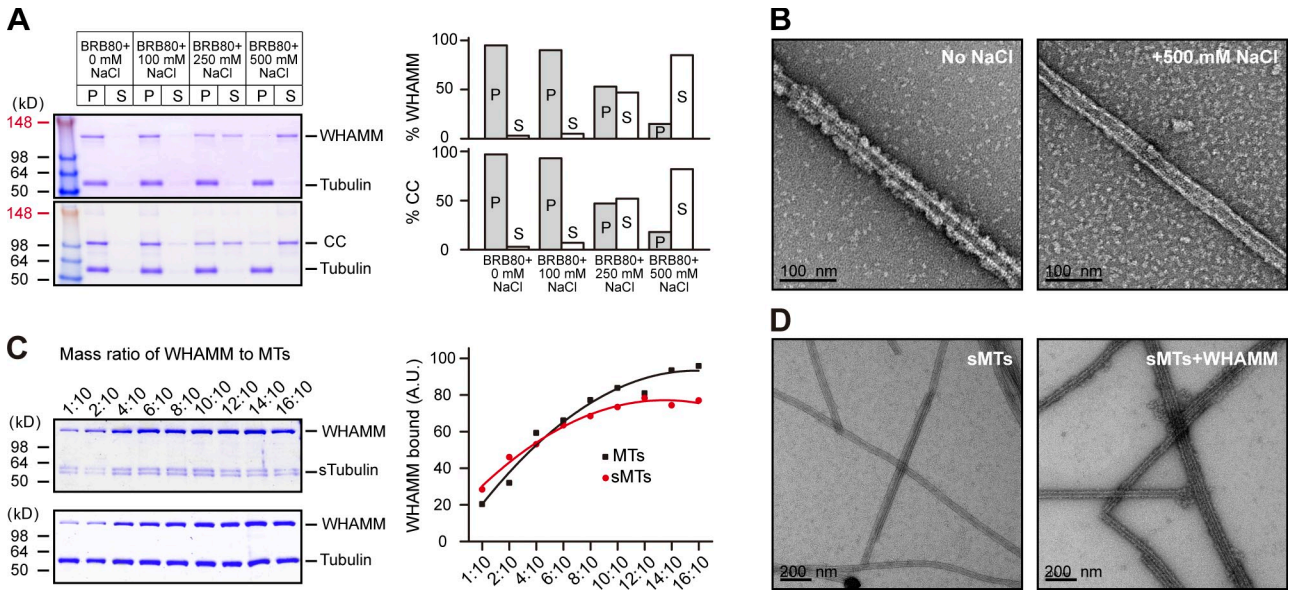

Figure 5. **Electrostatic interactions between the CC domain and α-tubulin E-hook play a key role in the assembly of WHAMM around MTs.** (A) MT cosedimentation assays were performed as in Fig. 1 but used 1 µM MBP-WHAMM or MBP-CC and 2 µM polymerized tubulin in the presence of different concentrations of NaCl. Densitometric quantifications of the Coomassie-stained gels are shown on the right. The data shown are from a single representative experiment out of three repeats. (B) Representative EM images of MTs incubated with MBP-WHAMM in 0 or 500 mM NaCl are shown. (C) MTs with or without subtilisin treatment were used in cosedimentation assays with different amounts of MBP-WHAMM. Pelleted WHAMM::MT complexes are shown in the gels on the left, and densitometric quantification is shown to the right. Cleavage of the E-hook of β-tubulin had minimal influence on the binding of WHAMM to MTs. The data are from a single representative experiment out of three repeats. The red line is the fitted curve of WHAMM to subtilisin-cleaved MTs (sMTs); the black line is the fitted curve of WHAMM to MTs as a control. (D) Representative EM images of nondecorated subtilisin-cleaved MTs (left) and MBP-WHAMM–decorated subtilisin-cleaved MTs (right) are shown. A.U. arbitrary unit; P, pellet; S, supernatant.

(PIPs), in vitro (Campellone et al., 2008), indicating that this portion of WHAMM is responsible for its membrane-binding function. Because the WMD appears to be surface exposed when WHAMM is bound to MTs, we next tested whether lipid vesicles could be recruited by WHAMM::MT complexes. To do this, we generated rhodamine-labeled liposomes from liver extract lipids (which are rich in ER- and Golgi-associated PIPs; Keenan and Morré, 1970), mixed them with WHAMM::MT complexes, and performed modified cosedimentation assays in which we measured the amount of rhodamine fluorescence in the pellet fractions. Interestingly, liver lipid–derived liposomes, but not DOPC (1,2-dioleoyl-*sn*-glycero-3-phosphocholine) liposomes (phosphocholine without PIPs), associated with the WHAMM::MT complexes in a dose-dependent manner and irrespective of the MBP tag (Fig. 6 A). MT binding required the WMD because liver lipid–derived liposomes also bound to WMD-CC::MT complexes but not CC::MT complexes or naked MTs (Fig. 6 A).

To visualize liposome recruitment by WHAMM-associated MTs, we formed WHAMM::MT complexes using green fluorescent MTs and examined the localization of rhodamine-labeled liposomes in a mixture with the WHAMM::MT complexes by fluorescence microscopy. In accordance with cosedimentation experiments, these microscopic analyses revealed that the liver lipid vesicles localized specifically at the surface of WHAMM-decorated MTs and not with CC-decorated or naked MTs (Fig. 6 B and not depicted). Thus, when WHAMM is bound to an MT, its WMD appears to be presented on the surface of protofilaments in a conformation compatible with its phospholipid-binding function.

To examine the liposomes that associated with the WHAMM::MT complex at higher resolution in their native shapes, we next investigated their morphology using cryo-EM. In agreement with the fluorescence microscopy results, we only saw liposomes made from liver extract lipids attach to WHAMM::MT complexes (Fig. 6 B). Interestingly, when we used liposomes of increased size (from an average diameter of 100–200 nm), we could visualize elongated membrane structures on the WHAMM::MT surface (Fig. 6 C), whereas unattached liposomes remained spherical (Fig. 6 B and Fig. S5 B). Even though we could not see the WHAMM protein between the liposomes and the MTs very clearly, the sharp shape of the ends of some liposomes (Fig. 6 C and Fig. S5 C) implied that WHAMM anchored the membrane tightly to the MT. Such a phenomenon was not detected in control samples using CC::MT complexes or naked MTs. Collectively, these results suggest that WHAMM::MT complexes are not only sufficient for recruiting vesicles but that they might also deform them into more elongated membranes.

MT binding decreases the actin nucleation activity of WHAMM

Although the peripheral density in our 3D map of the WHAMM::MT complex appears to be primarily composed of the WMD, the complex also included a smaller density that was more closely apposed to the MT attachment point of the CC domain. We speculated that this density might include the PWCA domain. Because this portion of WHAMM provides its NPF function, we tested whether MTs could affect the ability of WHAMM to stimulate Arp2/3-mediated actin assembly in vitro

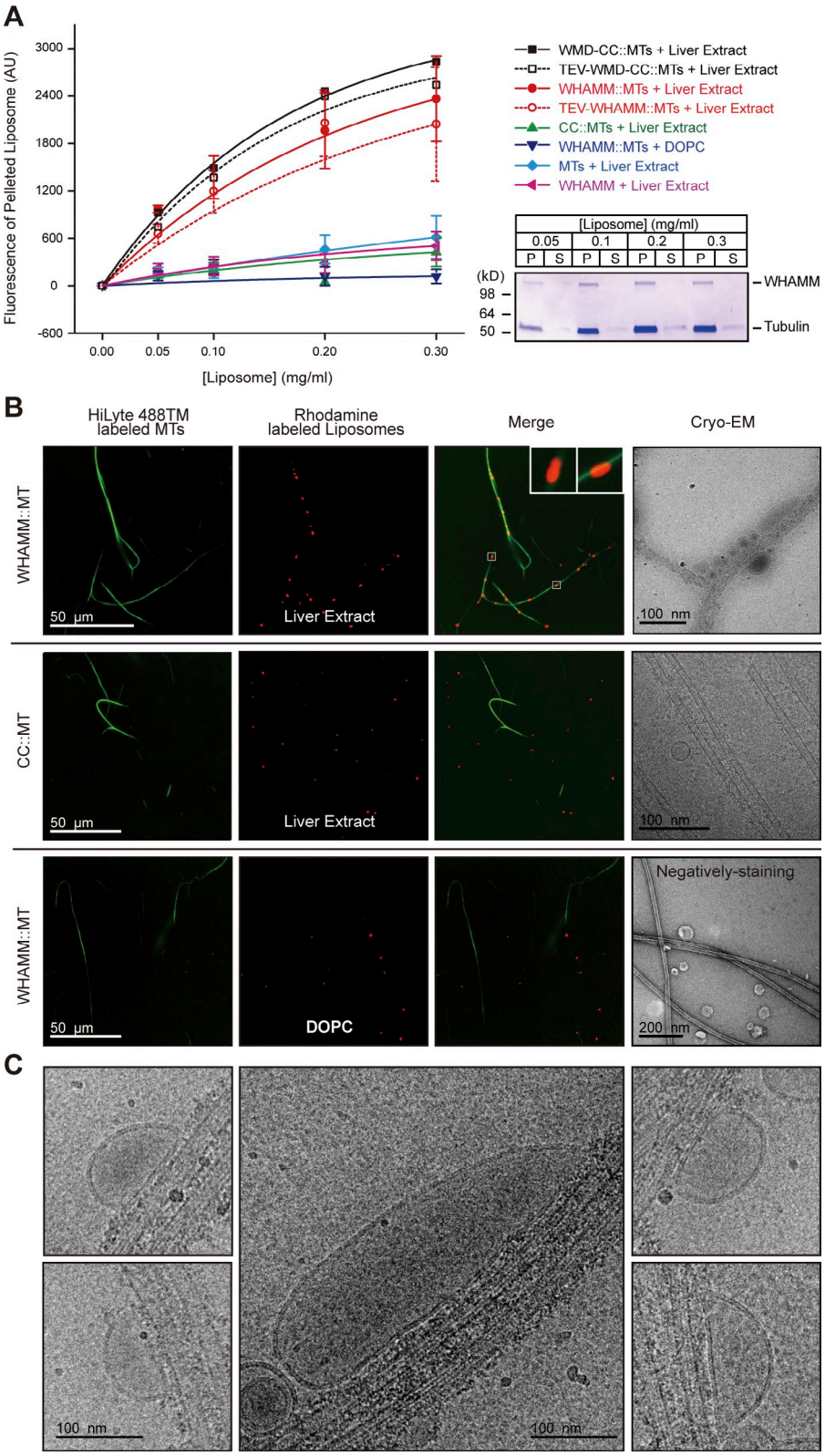

Figure 6. **MT-bound WHAMM can recruit and remodel membranes.** (A) Cosedimentation assays were performed using the indicated MT complexes and different concentrations of rhodamine-labeled liposomes generated from liver extract lipids. The amount of liposomes associated with MT pellets was measured in arbitrary units (AU) by quantifying the fluorescence at 590 nm (left), whereas the proper distribution of WHAMM and tubulin was confirmed by SDS-PAGE (bottom right). Where indicated, the MBP moiety was cleaved from WHAMM::MT complexes using the TEV protease. Error bars show the range of data, which is calculated by subtracting the lowest value from the highest value. (B) Green fluorescent MTs coated with MBP-WHAMM or MBP-CC were mixed with red fluorescent liposomes made from liver extracts or pure DOPC and examined by fluorescence or EM. Liver liposomes associated specifically with MTs coated with the full-length WHAMM protein and are highlighted in the inset images. (C) Typical cryo-EM images of MBP-WHAMM::MT complexes that recruited and deformed vesicles of different sizes are shown. P, pellet; S, supernatant.

by performing pyrene-actin polymerization assays in the absence or presence of MTs.

As expected, actin assembled slowly in reactions containing the Arp2/3 complex alone and rapidly in reactions containing Arp2/3 plus either full-length WHAMM or the WHAMM PWCA domain (Fig. 7 A). Interestingly, when reactions containing Arp2/3 and full-length WHAMM were performed in the presence of MTs, actin assembled at a much slower rate (Fig. 7 A). A decrease in actin polymerization rate was also observed when WHAMM was preincubated with MTs before it was mixed with Arp2/3 (Fig. 7 A). These results were confirmed by measuring the actin assembly rates when reactions reached half-maximal

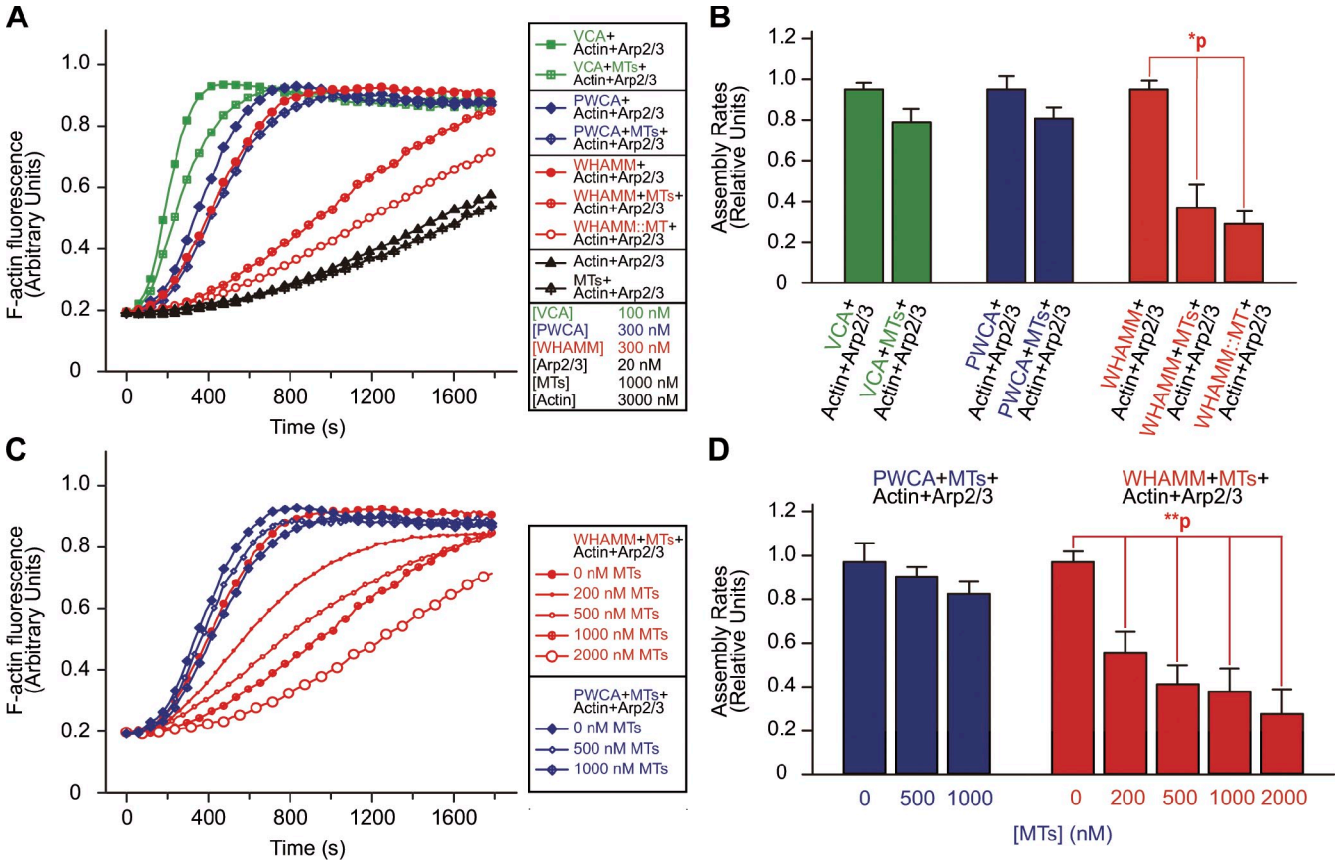

Figure 7. **MT binding decreases the actin nucleation-promoting activity of WHAMM.** (A) Actin (10% pyrene labeled) was polymerized in the presence of 20 nM Arp2/3 complex alone or in reactions that contained Arp2/3 plus the indicated concentrations of the GST-tagged VCA domain of WASP, MBP-tagged PWCA domain of WHAMM, or MBP-tagged full-length WHAMM. Reactions were performed in the absence (filled symbols) or presence of 1 µM MTs (hatched or open symbols). MBP-WHAMM that was added to polymerization reactions at the same time as MTs is denoted WHAMM + MTs + Actin + Arp2/3, whereas MBP-WHAMM that was preincubated with MTs for 30 min is labeled WHAMM::MT + Actin + Arp2/3 in the legend. (B) Relative assembly rates were calculated based on the slopes of polymerization curves at half-maximal polymer. For each Arp2/3 activator, the assembly rate without MTs was set to 1. Assembly rates in the presence of MTs were then calculated relative to the respective activator. WHAMM-mediated actin assembly was significantly slower in the presence of MTs than in their absence (*, $P = 1.5 \times 10^{-3}$). Neither VCA- nor PWCA-mediated actin assembly was significantly different when MTs were added ($P = 0.25$ and $P = 0.30$, respectively). (C) Actin was polymerized using the Arp2/3 complex plus 300 nM MBP-PWCA or MBP-WHAMM in the absence or presence of the indicated concentrations of MTs. (D) Relative assembly rates were calculated as in B. WHAMM-mediated actin assembly was significantly slower in the presence of MTs than in their absence (**, $P < 0.001$). Data represent the means ± SD from three experiments.

polymer (Fig. 7 B) and by measuring the dose dependence of the MT-mediated inhibitory effects (Fig. 7, C and D). In contrast to the observations that MTs reduce the NPF activity of full-length WHAMM, MTs used in ≤10-fold molar excess had little effect on the kinetics of actin polymerization driven by the PWCA domain of WHAMM or the WCA domain of a different NPF, WASP (Fig. 7, A–D). These latter findings indicate that MTs do not act as a general inhibitor of Arp2/3-mediated actin nucleation. Instead, the negative effect of MTs on actin assembly is specific to reactions containing full-length WHAMM molecules. Overall, our in vitro data point to a model in which engagement of a MT by the CC domain of WHAMM exposes the WMD to allow it to bind membranes but masks the PWCA domain to prevent it from activating the Arp2/3 complex.

Discussion

MTs and actin filaments orchestrate numerous cellular functions, yet relatively few molecules are known to physically interact with both cytoskeletal systems, and even less is understood about how the actions of such factors are coordinated. In this study, we describe a structural and biochemical basis for how WHAMM—a mammalian factor that influences membrane tubulation and transport—coordinates three fundamental activities: MT binding, membrane association, and actin nucleation. Our results therefore begin to unravel the mechanisms by which the MT and actin cytoskeletons influence one another during membrane remodeling.

Thus far, the best-characterized molecules that both function in actin nucleation and bind to MTs are the mammalian formins mDia1, mDia2, and INF2 (Gaillard et al., 2011), although other formins can also interact with actin and MTs (Bartolini et al., 2008; Young and Copeland, 2010). Each of these proteins nucleates actin and facilitates elongation of unbranched filaments, but the potency of these activities varies greatly among individual formins (Chesarone et al., 2010). More recently, recombinant fragments of mDia1, mDia2, and INF2 were shown to bind MTs but with different affinities (dissociation

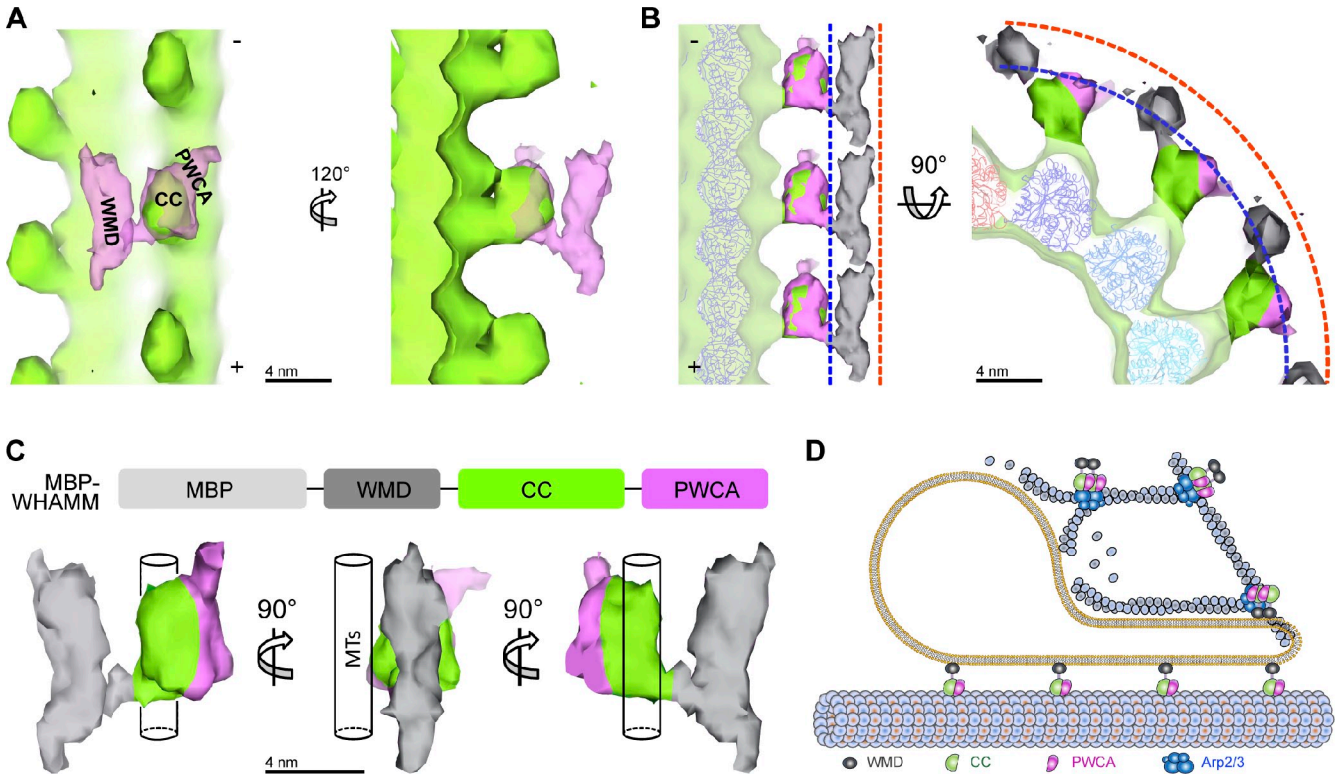

Figure 8. **The architecture of WHAMM-associated MTs gives rise to a working model for membrane tubulation.** (A) In this composite view of a WHAMM-coated MT, one MBP-WHAMM molecule (purple) is superimposed onto MBP-CC::MTs (green). The overlap density is depicted as the CC domain. The probable positions of the WMD and PWCA domains are also marked. (B) The WMD (gray) appears to be more peripherally located than the PWCA domain (pink) when WHAMM is bound to a MT. (C) A U-shaped architecture of WHAMM and its orientation with MTs are shown. The WMD is colored gray, CC is colored green, and PWCA is colored purple. (D) A hypothetical model depicts one population of WHAMM that can simultaneously bind to an MT (using its CC domain) and membrane tubule (using its peripheral WMD) but not actin or Arp2/3 (because it is hindered by nearby domains). Other non-MT–bound populations of WHAMM can likely link the membrane to actin and Arp2/3.

constants ranging from ∼50 nM to ∼2 µM) and with different stoichiometries (formin/tubulin ratios ranging from ∼2:1 to ∼1:3), depending on the identity of the formin and the truncation that was studied (Gaillard et al., 2011). Interestingly, MTs can inhibit the actin nucleation activity of mDia2 and mDia1 but not INF2 (Gaillard et al., 2011). However, it is not yet clear how full-length formin molecules engage MTs or how biochemical differences among the formins affect their membrane remodeling functions.

In contrast to the formins, the Arp2/3 complex—the only nucleator that causes both actin polymerization and branching—does not appear to interact with MTs. Somewhat surprisingly, aside from WHAMM, none of the mammalian WASP family NPFs have been shown to bind MTs. One of these, WASP and SCAR homologue (WASH), was demonstrated to interact with tubulin subunits in pull-down assays (Gomez and Billadeau, 2009), but it is not known whether this protein can actually bind to MT polymers. Interestingly, the distantly related WASP and WASH protein homologues in *Drosophila melanogaster* can associate with MTs (Liu et al., 2009), although the biochemical properties of these interactions have not been characterized.

For human WHAMM, we showed that recombinant versions of the full-length protein and its CC domain each bind to MTs with dissociation constants <500 nM and with 1:1 stoichiometry, indicating that WHAMM has a fairly high affinity for MTs and that this activity is likely contained entirely within its CC domain. However, the CC by itself had a higher affinity for MTs than the full-length protein did. It is not clear whether this twofold difference has functional significance, but it seems plausible that the PWCA portion of WHAMM masks the CC domain in the context of the full-length protein because a WHAMM construct lacking the PWCA region bound to MTs with an affinity similar to the CC domain by itself. Determining how the MT-binding properties of WHAMM are regulated intramolecularly and by other factors will require further analyses.

In spite of several key x-ray and nuclear magnetic resonance examinations of WASP family domain structures (Kim et al., 2000; Ti et al., 2011), as well as a more recent EM study (Xu et al., 2012), structural insights into the function of NPFs has generally lagged far behind the characterizations of their biochemical activities. Importantly, we report here that full-length WHAMM forms helical structures around MTs and solved this structure to an 18-Å resolution. Our 3D reconstruction of the WHAMM::MT complex and difference mapping based on the CC::MT complex (Fig. 8, A–C) revealed that WHAMM attaches to a MT in a U-shaped conformation, with WHAMM molecules assembled in a head to tail fashion along individual protofilaments and the CC domain linked to the outer ridge of a

tubulin heterodimer. This reconstruction appears to provide the first illustration of a CC region engaging an MT because among the dozens of MT-interacting proteins (Lyle et al., 2009a,b), none is known to physically associate with the MT using a CC domain. It remains to be seen whether the WHAMM CCs possess unique characteristics that allow them to bind to MTs or whether CCs from other proteins share this ability.

Other than its central CC domain, MT-bound WHAMM possesses two distinct densities: one closely associated with the CC fragment and a second with an elongated shape that is found at the periphery of the WHAMM::MT complex. We postulate that the exposed peripheral structure is mainly comprised of the phospholipid-binding WMD (Fig. 8, A–C). This idea is supported by the observation that WHAMM::MT complexes can recruit liposomes. The additional finding that liposomes are deformed when bound to WHAMM::MT complexes is also intriguing because some of these structures resemble the tubular membranes that are formed when WHAMM expression is increased in mammalian cells (Campellone et al., 2008). It is tempting to speculate that the organization of WHAMM along protofilaments may help membranes extend along the MT surface. In any case, our results give rise to a model in which individual WHAMM molecules act as direct physical links between MTs (bound via the CC domain) and cargo-carrying membranes (bound via the WMD; Fig. 8 D).

In addition to providing a view of how WHAMM simultaneously engages MTs and membranes, our 3D reconstructions imply that the PWCA domain is buried beneath the WMD and placed close to the CC domain when WHAMM is assembled around MTs (Fig. 8, A–C). This conformation is predicted to spatially hinder the association of the PWCA fragment with the actin nucleation machinery. In fact, when we performed pyrene-actin polymerization assays, we found that MTs specifically inhibit the nucleation function of WHAMM. Multiple mechanisms have been described for the suppression of NPF activity in WASP family proteins. Intramolecular autoinhibition controls WASP and neural WASP (Padrick and Rosen, 2010), whereas the WAVE isoforms (Derivery et al., 2009; Ismail et al., 2009; Lebensohn and Kirschner, 2009) and WASH are kept inactive by structurally related multisubunit complexes that bind to their N termini (Chen et al., 2010; Jia et al., 2010). Because WHAMM NPF activity does not appear to be autoinhibited (Campellone et al., 2008), we previously speculated that this activity would be suppressed in trans by WHAMM's binding partners (Campellone and Welch, 2010). However, it was still somewhat surprising to find that MTs act as one such regulator. Such an MT-based mechanism for controlling NPF activity provides individual WHAMM molecules with an ability to spatially separate their association with the two cytoskeletons.

Previous work indicated that both MTs and actin filaments are required for WHAMM-associated membrane tubulation and that Arp2/3-mediated actin assembly provides a force that drives tubule elongation (Campellone et al., 2008). But because the interaction between individual WHAMM molecules and MTs or Arp2/3 might be mutually exclusive, the MT-bound population of WHAMM probably collaborates with a distinct (non-MT associated) actin-nucleating population of WHAMM during the membrane tubulation process (Fig. 8 D). The fact that MT-bound WHAMM proteins are not active toward Arp2/3 ensures that the MTs are free from filamentous obstacles that might prevent membranes from spreading or moving along the MT surface. On the other hand, MT-independent WHAMM molecules could stimulate actin nucleation and branching to create forces that could deform a vesicle against the MT or promote its spread or motility along the MT.

Membrane remodeling is clearly essential for many cellular processes, especially vesicle trafficking and protein secretion, and a variety of proteins that operate by distinct mechanisms are known to influence membrane shape. These include the dynamin, BAR, ESCRT (endosomal sorting complex required for transport), and COP (coat protein) protein families, which use self-assembly properties to promote tubulation of their target membranes (Praefcke and McMahon, 2004; Frost et al., 2008; Hurley and Hanson, 2010; Zanetti et al., 2012). In addition, molecular motor proteins and their interaction partners can tubulate membranes by providing pulling forces along cytoskeletal polymers. The membrane tubulation that is driven by the coordinated MT binding and actin-nucleating activities of WHAMM represents another possible mechanism. It would not be surprising if the WHAMM-mediated process also involves some level of self-assembly as well as contributions from motor proteins and other factors. Future work aimed at identifying and characterizing these potential WHAMM-associated molecules should shed additional light on how the MT and actin cytoskeletons cooperate during membrane remodeling.

Materials and methods

Plasmids, bacteria, viruses, and cells

To generate large quantities of recombinant WHAMM proteins in a purified form, we developed a system that employs baculoviruses to drive expression of high levels of soluble MBP fusion proteins in insect cells. Past experience indicated that few WHAMM derivatives are expressed at high levels in *Escherichia coli*, irrespective of the identity of the host strain or of tagging with His, GST, or MBP moieties (Campellone et al., 2008). More recently, we found that MBP-WHAMM derivatives expressed in *Sf9* insect cells are abundant, soluble, and relatively easy to purify. To create the MBP expression vector pKC-FastBacMBP that was used in this study, the MBP-encoding gene *malE*, followed by a sequence encoding a TEV protease cleavage site, was cloned by PCR into the EcoRI and KpnI sites of the 6×His expression vector pKC-FastBac (Campellone et al., 2008). WHAMM derivatives encoding the full-length human protein (residues 1–809), a WMD-CC fragment (residues 1–630), the WMD (residues 1–260), the CC domain (residues 260–630), or the PWCA domain (residues 630–809) were inserted into pKC-FastBacMBP as KpnI–NotI fragments. Because pKC-FastBacMBP encodes a 6×His tag upstream of the *malE* sequence, all tagged proteins contain an N-terminal 6×His followed by MBP. Plasmids were maintained in *E. coli* XL1-Blue (Agilent Technologies), bacmids were generated in *E. coli* DH10 Bac, and baculoviruses were created using the Bac-to-Bac system (Invitrogen). The plasmid encoding His-CC contained the CC coding sequence as a KpnI–NotI fragment downstream of a 10×His tag in pKC-ET16b (Campellone et al., 2008). His-CC was expressed in *E. coli* BL21 Rosetta.

Protein purifications

Sf9 cells were grown in ESF921 medium (Expression Systems) and infected with baculoviruses encoding MBP fusion proteins at a multiplicity of infection of ∼1. Cells were freeze thawed, treated with permeabilization buffer (PB; 20 mM Tris, pH 7.6, 250 mM NaCl, 100 mM KCl, 1 mM DTT, 1 mM EDTA, 0.01% NP-40, 5% glycerol, 1 mM PMSF, and 10 µg/ml each of aprotinin, leupepstatin, pepstatin, and chymostatin), sonicated for 35 s four times, and subjected to a crushing spin for 22 min at 35,000 rpm at

4°C in a rotor (Ti-60; Beckman Coulter). To purify the MBP fusion proteins, supernatants were mixed with amylose resin (New England Biolabs, Inc.), and bound proteins were collected using elution buffer (EB; 20 mM Tris, pH 7.6, 250 mM NaCl, 100 mM KCl, 1 mM DTT, 1 mM EDTA, 5% glycerol, 10 mM maltose, 0.5 mM PMSF, and 5 µg/ml each of aprotinin, leupepstatin, pepstatin, and chymostatin). His-CC was isolated from *E. coli* using Ni-NTA affinity resin (QIAGEN) and eluted in 20 mM Tris buffer (20 mM Tris, pH 7.6, 250 mM NaCl, 100 mM KCl, and 1 mM DTT) containing 350 mM imidazole, similar to previously described His-tagged protein purifications (Campellone et al., 2008). All proteins were further purified and transferred into BRB80 buffer (80 mM Pipes, pH 6.8, 1 mM $MgCl_2$, and 1 mM EGTA) + 0.5 mM DTT ± KCl or NaCl using a gel filtration step (Superdex 200; GE Healthcare). The peak WHAMM-containing fractions were pooled, and small aliquots were frozen in liquid nitrogen and stored at −80°C. Protein quantities were measured using Bradford assays (Bio-Rad Laboratories, Inc.), and sample purity was confirmed by SDS-PAGE analyses.

Antibodies

Antibodies against MBP and WHAMM were generated by immunizing rabbits with purified MBP-WHAMM (Covance). Polyclonal anti-MBP antibodies were first affinity purified using MBP, and anti-WHAMM antibodies were subsequently affinity purified using MBP-WHAMM. The mouse antitubulin E7 antibody was obtained from the Developmental Studies Hybridoma Bank.

MT cosedimentation assays

Taxol-stabilized MTs were prepared from porcine brain tubulin as previously described elsewhere (Hyman et al., 1991). In brief, purified tubulin (6 mg/ml in BRB80 plus 1 mM DTT) was assembled into MTs in the presence of 2 mM GTP at 37°C for 30 min. To stabilize MT polymers, taxol was added in stepwise increments for another 30 min until a final concentration of 40 µM was reached. Fresh MTs were preferred for most experiments. Cleavage of the tubulin C terminus E-hook was performed by limited proteolysis of 1 mg/ml taxol-stabilized MTs using 1% (wt/wt) subtilisin (Knipling et al., 1999). The proteolysis reaction was stopped by adding freshly made 20 mM PMSF in DMSO. MTs or subtilisin-treated MTs were pelleted by ultracentrifugation at 60,000 *g* for 10 min and resuspended in BRB80 plus 0.5 mM DTT (and 20 mM PMSF in the case of the cleaved MTs) to the same concentration. For affinity and stoichiometry measurements, different ratios of MBP-WHAMM, MBP-WMD-CC, MBP-CC, or His-CC to MTs, quantified by Bradford assays, were mixed together at room temperature for 30 min and centrifuged at 60,000 *g* at 26°C for 10–20 min. Supernatants and pellets were adjusted to equivalent volumes and subjected to SDS-PAGE. For affinity experiments, SDS-PAGE gels were immunoblotted with rabbit anti-MBP antibodies and mouse antitubulin antibodies and visualized using HRP-conjugated secondary antibodies (GE Healthcare) or were detected by silver staining. To measure the amount of MBP-WHAMM derivatives that cosedimented with MTs, protein levels in pellet samples and in standards of known concentration were quantified by measuring pixel intensities with ImageJ software (National Institutes of Health). For stoichiometry experiments, the relative amounts of WHAMM proteins in the pellet versus supernatant fractions were quantified by staining with Coomassie brilliant blue and analyzing the band intensity densitometrically using the TotalLab (v.2.01) software program as previously described (Shen et al., 2009). At concentrations above a 1:1 WHAMM/tubulin heterodimer ratio, WHAMM proteins appeared in supernatant samples in a manner proportional to the molar excess of WHAMM that was used. Binding stoichiometry was also confirmed by comparing the intensity of WHAMM and tubulin bands in pellet samples.

Sample preparation for microscopic examination

2 µl WHAMM derivatives (1.2 mg/ml) were mixed with 8 µl taxol-stabilized MTs or subtilisin-cleaved MTs (0.1 mg/ml each) at room temperature for 30 min. The samples were diluted three times before being negatively stained by 2% (wt/vol) uranyl acetate solution on continuous carbon-coated copper grids or were directly frozen on Quantifoil grids under liquid nitrogen temperature using a vitrification device (Vitrobot; FEI). The negatively stained samples were examined under an electron microscope (Tecnai-12; FEI) operated at 120 kV and recorded on a charge-coupled device camera (Ultrascan4000; Gatan) at 46,000×. The frozen hydrated samples were examined under a microscope (Tecnai G^2 F20; FEI) with a field emission gun in low-dose mode under the accelerating voltage of 200 kV and a magnification of 34,000×. Micrographs were captured on a charge-coupled device camera (Ultrascan4000) with the final pixel size of 3.7 Å. For gold labeling assays, the formation of WHAMM::MT complexes was first confirmed by negative stain EM, and then, 2-nm Ni-NTA-gold particles were incubated with parallel samples containing WHAMM::MT or control MTs at room temperature for 30 min, and the mixtures were subjected to negative stain EM. For fluorescence microscopy, HiLyte Fluo 488–labeled tubulin (Cytoskeleton) was placed in the dark at 37°C for 60 min to form MTs. 2 µl WHAMM derivatives (1.2 mg/ml) were mixed with 8 µl taxol-stabilized HiLyte Fluo 488 MTs (0.1 mg/ml) at room temperature for 30 min. The decoration was checked by negative staining EM. Unilamellar liposomes were also prepared (Shen et al., 2009) and homogenized to different sizes by using an extruder (Mini-Extruder; Avanti Polar Lipids, Inc.) according to the manufacturer's instructions. 5% rhodamine-labeled DOPE (1,2-dioleoyl-*sn*-glycero-3-phosphatidylethanolamine; Avanti Polar Lipids, Inc.) was added to liver extract lipids or to pure DOPC and blown up to 100- or 200-nm liposomes. 1 µl rhodamine-labeled liposomes (0.5 mg/ml) was mixed with 10 µl of WHAMM/CC::MT (HiLyte Fluo 488) mixtures at room temperature for 60 min. The samples were treated with antifade reagent (ProLong; Invitrogen), and images were acquired using 40× water immersion objective lens on a confocal microscope (TCS SP2; Leica) with excitation at 488 nm and emission at 580 nm at room temperature. The images were then processed using ImageJ software. An extra 2 µl of the triple mixture was negatively stained or vitrified in liquid nitrogen temperature for further EM examination.

TEV cleavage assays

8 µl of MBP-WHAMM (1.2 mg/ml) or MBP-WMD-CC (1.2 mg/ml) derivative were mixed with 32 µl taxol-stabilized MTs (0.3 mg/ml) to form WHAMM::MT or WMD-CC::MT complexes at room temperature for 30 min. The samples were subjected to TEV cleavage assays in 60 µl volume at room temperature based on the manufacturer's protocol (Invitrogen). Twice as much TEV protease was needed to efficiently cleave WHAMM::MT. At different time points, 10-µl samples were removed and subjected to SDS-PAGE directly or were centrifuged at 60,000 *g* at 26°C for 10–20 min. Supernatants and pellets were adjusted to equivalent volumes before SDS-PAGE. The final cleaved WHAMM::MT and WMD-CC::MT complexes were negatively stained using 2% (wt/vol) uranyl acetate solution on continuous carbon-coated copper grids. The TEV protease cleavage of free MBP-WMD-CC was successfully performed under the same conditions, but cleavage of free MBP-WHAMM resulted in WHAMM precipitation in the initial buffers that we tested. 12 µl of cleaved soluble WMD-CC was mixed with 6.5 µl taxol-stabilized MTs (0.3 mg/ml) at room temperature for 30 min. The mixture was then subjected to negative staining or centrifuged to separate the pellets from supernatants.

Vesicle and MT cosedimentation assay

Freshly made 100-nm liposomes made from liver extract lipid or DOPC with 5% rhodamine-labeled DOPE were centrifuged at 18,000 *g* at room temperature to remove possible aggregates. Then, the liposomes at different final concentrations (0, 0.05, 0.1, 0.2, and 0.3 mg/ml) were mixed with WHAMM::MT or other complexes containing 5% glycerol (0.05 mg/ml final concentration) at room temperature for 30 min. The protein–vesicle complex was then centrifuged at 18,000 *g* for 10 min. Supernatants and pellets were adjusted to equivalent volumes and subjected to SDS-PAGE to confirm the sedimentation of MTs and WHAMM proteins. The distribution of liposomes was measured by reading the fluorescence at 590 nm using a fluorometric plate reader (Microplate Reader; Tecan). The use of different dilutions of both supernatants and pellets guaranteed that all data points were readable, and standard liposome fluorescence curves were used to calculate the amount of vesicles in the pellets.

Image analyses and 3D reconstructions

The Helixboxer program in the EMAN image processing suite was used to box WHAMM::MT filaments and to perform fast Fourier transform (FFT) analysis (Ludtke et al., 1999). Only those fully decorated WHAMM::MT filaments with good FFT signals were used for further processing. Their 1D projection profiles were processed on a Linux PC using SUPRIM software (Schroeter and Bretaudiere, 1996). The WHAMM::MT or His-CC::MT filaments were boxed by EMAN in helical mode with 90% overlap to generate single-particle images. The single particles were subjected to 2D alignment and classification in IMAGIC software package obtained from Image Science Software GmbH (van Heel et al., 1996).

3D helical refinements and reconstructions of WHAMM::MT or His-CC::MT adopted the same strategy as kinesin::MT complexes with some modifications (Sindelar and Downing, 2007, 2010). The kinesin::MT structure was filtered to 30 Å as the initial reference to align the raw images. Based on the alignment analysis, only 13-protofilament MTs were screened

for further use. After reference-based alignments were derived for the contrast transfer function corrected MT segments, pseudosymmetry transforms were applied to merge all tubulin heterodimer subunits (with contrast transfer function correction) into a 3D volume describing a single correctly averaged protofilament using the FREALIGN algorithm as described previously (Grigorieff, 2007; Alushin et al., 2010); this "good" protofilament was subsequently replicated and transformed by real-space symmetry operators to generate a complete three-start, 13-protofilament MT map using a SPIDER script (Sindelar and Downing, 2007, 2010). After six cycles of FREALIGN refinement and reconstruction, the reconstructed MT volume was filtered to a 16-Å resolution and used to generate a new set of reference images for a second round of SPIDER script refinement followed by six cycles of FREALIGN refinement/reconstruction. After these steps, the refinements were judged to have converged based on observed resolution statistics.

For WHAMM::MT complexes, the final volume incorporated 88 micrographs, representing 235 MTs for a total of 8,186 unique image segments. The final resolution was estimated to be ∼18 Å using both RMEASURE (Sousa and Grigorieff, 2007) and the Fourier shell correlation (0.5 criterion). For His-CC::MT complexes, the final volume involved 77 micrographs, representing 216 MTs for a total of 6,265 unique image segments. The final resolution was estimated to be 22 Å. The difference map between WHAMM::MT and His-CC::MT was calculated using Matlab 2011b software (MathWorks) with an in-house script (supplemental material). The docking of MT atomic model (Protein Data Bank accession no. 1JFF; Li et al., 2002) was performed in the University of California, San Francisco Chimera with the fit model in map function (Pettersen et al., 2004). The Electron Microscopy Data Bank accession numbers for WHAMM::MT and CC::MT 3D reconstructions are EMD-2157 and EMD-5463, respectively.

Pyrene-actin assembly assays

Rabbit skeletal muscle actin, pyrene-actin, WASP GST-VCA (Verprolin, cofilin, and acidic), and bovine Arp2/3 complex were purchased from Cytoskeleton. Assembly assays performed in the absence of MTs were performed essentially as previously described (Goley et al., 2004). In brief, 3 µM actin (containing 10% pyrene-actin) was polymerized in the presence of 20 nM Arp2/3 complex with or without its regulators. GST-VCA was used at a final concentration of 100 nM, whereas MBP-WHAMM and MBP-PWCA were used at 300 nM each. To examine the effects of MTs on actin assembly kinetics, MTs (used at final concentrations of 200–2,000 nM) were mixed with the WASP or WHAMM proteins immediately before actin polymerization reactions were initiated. In some experiments, MTs were incubated with the WASP or WHAMM proteins at room temperature for 30 min before actin polymerization reactions were initiated. The decoration of WHAMM around MTs and actin branching was confirmed by negative stain EM. Relative actin assembly rates were calculated by measuring the slopes of pyrene curves at half of the maximal F-actin concentration. Statistical comparisons were made using a *t* test in Excel (Microsoft).

Online supplemental material

Fig. S1 shows the 2D class averages of WHAMM on MTs and their respective power spectrums. Fig. S2 shows the MT-binding properties of uncleaved and cleaved versions of MBP-WMD-CC. Fig. S3 shows the 2D class averages and helical structures of CC on MTs. Fig. S4 shows the resolution estimation and unbiased reference character of the WHAMM::MT complex reconstruction. Fig. S5 shows the accessibility of the N-terminal His tag of WHAMM when bound to MTs in addition to galleries of normal spherical liposomes and deformed liposomes bound to WHAMM::MT complexes. A supplemental file is also provided that contains the Matlab script for calculating the difference map between two 3D reconstructions. Online supplemental material is available at http://www.jcb.org/cgi/content/full/jcb.201204010/DC1.

We thank Prof. Thomas Pollard and Dr. Qian Chen at Yale Department of Molecular, Cellular, and Developmental Biology for comments on the manuscript and actin polymerization assays. We thank the Yale Center for Cellular and Molecular Imaging facility, Cryo-EM facility, High-Performance Computing facility, Prof. Jim Rothman, Prof. Frédéric Pincet, Dr. Lei Shi, and Dr. Weiming Xu for kindly providing us with the necessary instruments. We also thank Jon Soderholm and Rebecca Heald at the University of California, Berkeley for providing purified tubulin samples.

H.-W. Wang is a recipient of the Smith Family Award for Excellence in Biomedical Research. K.G. Campellone was supported by a Leukemia and Lymphoma Society Career Development Fellowship and by the University of Connecticut Research Foundation.

Submitted: 3 April 2012
Accepted: 3 September 2012

References

Alushin, G.M., V.H. Ramey, S. Pasqualato, D.A. Ball, N. Grigorieff, A. Musacchio, and E. Nogales. 2010. The Ndc80 kinetochore complex forms oligomeric arrays along microtubules. *Nature*. 467:805–810. http://dx.doi.org/10.1038/nature09423

Bartolini, F., J.B. Moseley, J. Schmoranzer, L. Cassimeris, B.L. Goode, and G.G. Gundersen. 2008. The formin mDia2 stabilizes microtubules independently of its actin nucleation activity. *J. Cell Biol.* 181:523–536. http://dx.doi.org/10.1083/jcb.200709029

Brownhill, K., L. Wood, and V. Allan. 2009. Molecular motors and the Golgi complex: staying put and moving through. *Semin. Cell Dev. Biol.* 20:784–792. http://dx.doi.org/10.1016/j.semcdb.2009.03.019

Campellone, K.G., and M.D. Welch. 2010. A nucleator arms race: cellular control of actin assembly. *Nat. Rev. Mol. Cell Biol.* 11:237–251. http://dx.doi.org/10.1038/nrm2867

Campellone, K.G., N.J. Webb, E.A. Znameroski, and M.D. Welch. 2008. WHAMM is an Arp2/3 complex activator that binds microtubules and functions in ER to Golgi transport. *Cell*. 134:148–161. http://dx.doi.org/10.1016/j.cell.2008.05.032

Chen, Z., D. Borek, S.B. Padrick, T.S. Gomez, Z. Metlagel, A.M. Ismail, J. Umetani, D.D. Billadeau, Z. Otwinowski, and M.K. Rosen. 2010. Structure and control of the actin regulatory WAVE complex. *Nature*. 468:533–538. http://dx.doi.org/10.1038/nature09623

Chesarone, M.A., A.G. DuPage, and B.L. Goode. 2010. Unleashing formins to remodel the actin and microtubule cytoskeletons. *Nat. Rev. Mol. Cell Biol.* 11:62–74. http://dx.doi.org/10.1038/nrm2816

Derivery, E., B. Lombard, D. Loew, and A. Gautreau. 2009. The Wave complex is intrinsically inactive. *Cell Motil. Cytoskeleton*. 66:777–790. http://dx.doi.org/10.1002/cm.20342

Dumont, S., and T.J. Mitchison. 2009. Force and length in the mitotic spindle. *Curr. Biol.* 19:R749–R761. http://dx.doi.org/10.1016/j.cub.2009.07.028

Ferguson, S.M., and P. De Camilli. 2012. Dynamin, a membrane-remodelling GTPase. *Nat. Rev. Mol. Cell Biol.* 13:75–88.

Frost, A., R. Perera, A. Roux, K. Spasov, O. Destaing, E.H. Egelman, P. De Camilli, and V.M. Unger. 2008. Structural basis of membrane invagination by F-BAR domains. *Cell*. 132:807–817. http://dx.doi.org/10.1016/j.cell.2007.12.041

Gaillard, J., V. Ramabhadran, E. Neumanne, P. Gurel, L. Blanchoin, M. Vantard, and H.N. Higgs. 2011. Differential interactions of the formins INF2, mDia1, and mDia2 with microtubules. *Mol. Biol. Cell*. 22:4575–4587. http://dx.doi.org/10.1091/mbc.E11-07-0616

Galletta, B.J., O.L. Mooren, and J.A. Cooper. 2010. Actin dynamics and endocytosis in yeast and mammals. *Curr. Opin. Biotechnol.* 21:604–610. http://dx.doi.org/10.1016/j.copbio.2010.06.006

Gatlin, J.C., and K. Bloom. 2010. Microtubule motors in eukaryotic spindle assembly and maintenance. *Semin. Cell Dev. Biol.* 21:248–254. http://dx.doi.org/10.1016/j.semcdb.2010.01.015

Goley, E.D., S.E. Rodenbusch, A.C. Martin, and M.D. Welch. 2004. Critical conformational changes in the Arp2/3 complex are induced by nucleotide and nucleation promoting factor. *Mol. Cell*. 16:269–279. http://dx.doi.org/10.1016/j.molcel.2004.09.018

Gomez, T.S., and D.D. Billadeau. 2009. A FAM21-containing WASH complex regulates retromer-dependent sorting. *Dev. Cell*. 17:699–711. http://dx.doi.org/10.1016/j.devcel.2009.09.009

Grigorieff, N. 2007. FREALIGN: high-resolution refinement of single particle structures. *J. Struct. Biol.* 157:117–125. http://dx.doi.org/10.1016/j.jsb.2006.05.004

Harrison, B.C., S.P. Marchese-Ragona, S.P. Gilbert, N. Cheng, A.C. Steven, and K.A. Johnson. 1993. Decoration of the microtubule surface by one kinesin head per tubulin heterodimer. *Nature*. 362:73–75. http://dx.doi.org/10.1038/362073a0

Hu, J., W.A. Prinz, and T.A. Rapoport. 2011. Weaving the web of ER tubules. *Cell*. 147:1226–1231. http://dx.doi.org/10.1016/j.cell.2011.11.022

Hurley, J.H., and P.I. Hanson. 2010. Membrane budding and scission by the ESCRT machinery: it's all in the neck. *Nat. Rev. Mol. Cell Biol.* 11:556–566. http://dx.doi.org/10.1038/nrm2937

Hyman, A., D. Drechsel, D. Kellogg, S. Salser, K. Sawin, P. Steffen, L. Wordeman, and T. Mitchison. 1991. Preparation of modified tubulins. *Methods Enzymol.* 196:478–485. http://dx.doi.org/10.1016/0076-6879(91)96041-O

Ismail, A.M., S.B. Padrick, B. Chen, J. Umetani, and M.K. Rosen. 2009. The WAVE regulatory complex is inhibited. *Nat. Struct. Mol. Biol.* 16:561–563. http://dx.doi.org/10.1038/nsmb.1587

Jia, D., T.S. Gomez, Z. Metlagel, J. Umetani, Z. Otwinowski, M.K. Rosen, and D.D. Billadeau. 2010. WASH and WAVE actin regulators of the Wiskott-Aldrich syndrome protein (WASP) family are controlled by analogous structurally related complexes. *Proc. Natl. Acad. Sci. USA*. 107:10442–10447. http://dx.doi.org/10.1073/pnas.0913293107

Kaksonen, M., C.P. Toret, and D.G. Drubin. 2006. Harnessing actin dynamics for clathrin-mediated endocytosis. *Nat. Rev. Mol. Cell Biol.* 7:404–414. http://dx.doi.org/10.1038/nrm1940

Keenan, T.W., and D.J. Morré. 1970. Phospholipid class and fatty acid composition of golgi apparatus isolated from rat liver and comparison with other cell fractions. *Biochemistry*. 9:19–25. http://dx.doi.org/10.1021/bi00803a003

Kim, A.S., L.T. Kakalis, N. Abdul-Manan, G.A. Liu, and M.K. Rosen. 2000. Autoinhibition and activation mechanisms of the Wiskott-Aldrich syndrome protein. *Nature*. 404:151–158. http://dx.doi.org/10.1038/35004513

Knipling, L., J. Hwang, and J. Wolff. 1999. Preparation and properties of pure tubulin S. *Cell Motil. Cytoskeleton*. 43:63–71. http://dx.doi.org/10.1002/(SICI)1097-0169(1999)43:1<63::AID-CM7>3.0.CO;2-Z

Lakämper, S., and E. Meyhöfer. 2005. The E-hook of tubulin interacts with kinesin's head to increase processivity and speed. *Biophys. J.* 89:3223–3234. http://dx.doi.org/10.1529/biophysj.104.057505

Lebensohn, A.M., and M.W. Kirschner. 2009. Activation of the WAVE complex by coincident signals controls actin assembly. *Mol. Cell*. 36:512–524. http://dx.doi.org/10.1016/j.molcel.2009.10.024

Li, H., D.J. DeRosier, W.V. Nicholson, E. Nogales, and K.H. Downing. 2002. Microtubule structure at 8 A resolution. *Structure*. 10:1317–1328. http://dx.doi.org/10.1016/S0969-2126(02)00827-4

Liu, R., M.T. Abreu-Blanco, K.C. Barry, E.V. Linardopoulou, G.E. Osborn, and S.M. Parkhurst. 2009. Wash functions downstream of Rho and links linear and branched actin nucleation factors. *Development*. 136:2849–2860. http://dx.doi.org/10.1242/dev.035246

Lowe, M. 2011. Structural organization of the Golgi apparatus. *Curr. Opin. Cell Biol.* 23:85–93. http://dx.doi.org/10.1016/j.ceb.2010.10.004

Ludtke, S.J., P.R. Baldwin, and W. Chiu. 1999. EMAN: semiautomated software for high-resolution single-particle reconstructions. *J. Struct. Biol.* 128:82–97. http://dx.doi.org/10.1006/jsbi.1999.4174

Lyle, K., P. Kumar, and T. Wittmann. 2009a. SnapShot: Microtubule Regulators I. *Cell*. 136:380, 380.e1.

Lyle, K., P. Kumar, and T. Wittmann. 2009b. SnapShot: Microtubule regulators II. *Cell*. 136:566, 566.e1.

Padrick, S.B., and M.K. Rosen. 2010. Physical mechanisms of signal integration by WASP family proteins. *Annu. Rev. Biochem.* 79:707–735. http://dx.doi.org/10.1146/annurev.biochem.77.060407.135452

Pettersen, E.F., T.D. Goddard, C.C. Huang, G.S. Couch, D.M. Greenblatt, E.C. Meng, and T.E. Ferrin. 2004. UCSF Chimera—a visualization system for exploratory research and analysis. *J. Comput. Chem.* 25:1605–1612. http://dx.doi.org/10.1002/jcc.20084

Polishchuk, R.S., M. Capestrano, and E.V. Polishchuk. 2009. Shaping tubular carriers for intracellular membrane transport. *FEBS Lett.* 583:3847–3856. http://dx.doi.org/10.1016/j.febslet.2009.10.031

Pollard, T.D., and J.A. Cooper. 2009. Actin, a central player in cell shape and movement. *Science*. 326:1208–1212. http://dx.doi.org/10.1126/science.1175862

Praefcke, G.J., and H.T. McMahon. 2004. The dynamin superfamily: universal membrane tubulation and fission molecules? *Nat. Rev. Mol. Cell Biol.* 5:133–147. http://dx.doi.org/10.1038/nrm1313

Qualmann, B., D. Koch, and M.M. Kessels. 2011. Let's go bananas: revisiting the endocytic BAR code. *EMBO J.* 30:3501–3515. http://dx.doi.org/10.1038/emboj.2011.266

Ramabhadran, V., F. Korobova, G.J. Rahme, and H.N. Higgs. 2011. Splice variant-specific cellular function of the formin INF2 in maintenance of Golgi architecture. *Mol. Biol. Cell*. 22:4822–4833. http://dx.doi.org/10.1091/mbc.E11-05-0457

Ramey, V.H., H.W. Wang, Y. Nakajima, A. Wong, J. Liu, D. Drubin, G. Barnes, and E. Nogales. 2011a. The Dam1 ring binds to the E-hook of tubulin and diffuses along the microtubule. *Mol. Biol. Cell*. 22:457–466. http://dx.doi.org/10.1091/mbc.E10-10-0841

Ramey, V.H., A. Wong, J. Fang, S. Howes, G. Barnes, and E. Nogales. 2011b. Subunit organization in the Dam1 kinetochore complex and its ring around microtubules. *Mol. Biol. Cell*. 22:4335–4342. http://dx.doi.org/10.1091/mbc.E11-07-0659

Redeker, V., R. Melki, D. Promé, J.P. Le Caer, and J. Rossier. 1992. Structure of tubulin C-terminal domain obtained by subtilisin treatment. The major alpha and beta tubulin isotypes from pig brain are glutamylated. *FEBS Lett.* 313:185–192. http://dx.doi.org/10.1016/0014-5793(92)81441-N

Saraste, J., H.A. Dale, S. Bazzocco, and M. Marie. 2009. Emerging new roles of the pre-Golgi intermediate compartment in biosynthetic-secretory trafficking. *FEBS Lett.* 583:3804–3810. http://dx.doi.org/10.1016/j.febslet.2009.10.084

Schroeter, J.P., and J.P. Bretaudiere. 1996. SUPRIM: easily modified image processing software. *J. Struct. Biol.* 116:131–137. http://dx.doi.org/10.1006/jsbi.1996.0021

Shen, Q.T., X.C. Bai, L.F. Chang, Y. Wu, H.W. Wang, and S.F. Sui. 2009. Bowl-shaped oligomeric structures on membranes as DegP's new functional forms in protein quality control. *Proc. Natl. Acad. Sci. USA*. 106:4858–4863. http://dx.doi.org/10.1073/pnas.0811780106

Shibata, Y., J. Hu, M.M. Kozlov, and T.A. Rapoport. 2009. Mechanisms shaping the membranes of cellular organelles. *Annu. Rev. Cell Dev. Biol.* 25:329–354. http://dx.doi.org/10.1146/annurev.cellbio.042308.113324

Sindelar, C.V., and K.H. Downing. 2007. The beginning of kinesin's force-generating cycle visualized at 9-Å resolution. *J. Cell Biol.* 177:377–385. http://dx.doi.org/10.1083/jcb.200612090

Sindelar, C.V., and K.H. Downing. 2010. An atomic-level mechanism for activation of the kinesin molecular motors. *Proc. Natl. Acad. Sci. USA*. 107:4111–4116. http://dx.doi.org/10.1073/pnas.0911208107

Sousa, D., and N. Grigorieff. 2007. Ab initio resolution measurement for single particle structures. *J. Struct. Biol.* 157:201–210. http://dx.doi.org/10.1016/j.jsb.2006.08.003

Ti, S.C., C.T. Jurgenson, B.J. Nolen, and T.D. Pollard. 2011. Structural and biochemical characterization of two binding sites for nucleation-promoting factor WASp-VCA on Arp2/3 complex. *Proc. Natl. Acad. Sci. USA*. 108:E463–E471. http://dx.doi.org/10.1073/pnas.1100125108

van Heel, M., G. Harauz, E.V. Orlova, R. Schmidt, and M. Schatz. 1996. A new generation of the IMAGIC image processing system. *J. Struct. Biol.* 116:17–24. http://dx.doi.org/10.1006/jsbi.1996.0004

Wang, H.W., and E. Nogales. 2005. Nucleotide-dependent bending flexibility of tubulin regulates microtubule assembly. *Nature*. 435:911–915. http://dx.doi.org/10.1038/nature03606

Wendt, T.G., N. Volkmann, G. Skiniotis, K.N. Goldie, J. Müller, E. Mandelkow, and A. Hoenger. 2002. Microscopic evidence for a minus-end-directed power stroke in the kinesin motor ncd. *EMBO J.* 21:5969–5978. http://dx.doi.org/10.1093/emboj/cdf622

Xu, X.P., I. Rouiller, B.D. Slaughter, C. Egile, E. Kim, J.R. Unruh, X. Fan, T.D. Pollard, R. Li, D. Hanein, and N. Volkmann. 2012. Three-dimensional reconstructions of Arp2/3 complex with bound nucleation promoting factors. *EMBO J.* 31:236–247. http://dx.doi.org/10.1038/emboj.2011.343

Yang, C., L. Czech, S. Gerboth, S. Kojima, G. Scita, and T. Svitkina. 2007. Novel roles of formin mDia2 in lamellipodia and filopodia formation in motile cells. *PLoS Biol.* 5:e317. http://dx.doi.org/10.1371/journal.pbio.0050317

Young, K.G., and J.W. Copeland. 2010. Formins in cell signaling. *Biochim. Biophys. Acta*. 1803:183–190. http://dx.doi.org/10.1016/j.bbamcr.2008.09.017

Zanetti, G., K.B. Pahuja, S. Studer, S. Shim, and R. Schekman. 2012. COPII and the regulation of protein sorting in mammals. *Nat. Cell Biol.* 14:20–28. http://dx.doi.org/10.1038/ncb2390

Zanic, M., J.H. Stear, A.A. Hyman, and J. Howard. 2009. EB1 recognizes the nucleotide state of tubulin in the microtubule lattice. *PLoS ONE.* 4:e7585. http://dx.doi.org/10.1371/journal.pone.0007585